Monitoring atmospheric phenomena on Titan

M. Hirtzig[1], A. Coustenis[1], E. Gendron[1], P. Drossart[1], A. Negrão[1,3], M. Combes[1], O. Lai[1,2], P. Rannou[3] and S. Lebonnois[4]

[1] LESIA, Observatoire de Paris-Meudon, 92195 Meudon Cedex, France
   e-mail: `mathieu.hirtzig@obspm.fr`
[2] CFHT, Hawaii
   e-mail: `lai@cfht.hawaii.edu`
[3] S.A. and Univ. de Versailles, France

[4] L.M.D., Jussieu, 75252 Paris Cx 05, France

Abstract. Titan's atmosphere, currently scrutinized in situ by the Cassini-Huygens mission, exhibits at the current era variations or new apparitions of atmospheric phenomena, that we have studied with adaptive optics imaging for the past 6 years. They include seasonal and diurnal effects, as well as some very interesting features in the South polar region. Some of these features have been interpreted as tropospheric transient clouds. Some of them have been observed in the past few years, since 2001, in adaptive optics with large ground-based telescopes such as the Keck, the VLT and CFHT. The latter two telescopes, with the instruments NACO and PUEO respectively, were used by our team in the current study, pertaining to data recorded from 1998 to 2005. The North-South Asymmetry (NSA) is shown to have changed since 2000 in the near-IR and to be currently organized in a brighter northern than southern pole. We study here this evolution. From our data, it also appears that diurnal effects indeed exist in Titan's stratosphere, with a brighter morning limb appearing in our images in many cases, when the phase effect is on the evening side. The southern bright revolving feature can not be attributed to the surface. It is a meteorological phenomenon, revolving around the South pole (confined in its motion within the 80°S parallel) located in the upper troposphere. Its behaviour and possible nature are discussed here.

Key words. Planets and satellites: individual:Titan – Instrumentation: adaptive optics – infrared : solar system

1. Introduction

We have observed Titan with five different adaptive optics systems from 1994 to 2005, monitoring surface and atmospheric features (Combes et al., 1997; Coustenis et al., 2001; Gendron et al., 2004; Hirtzig et al., 2005; Coustenis et al., 2005a). In the past 4 years we have performed imaging with NAOS/CONICA (NACO) at the Very Large Telescope (Yepun, 8-m, Chili) and with PUEO at the Canada France Hawaii Telescope (3.6-m, Hawaii) in order to characterize the surface and the atmosphere of the satellite. Our findings in terms of the surface properties are described in Coustenis et al. (2005a). In this paper we focus on the information that we have gathered by investigating chronologically the atmospheric features seen in our images. Our observations as a whole are summarized in Table 1.

The filters we have used to probe Titan's atmosphere and surface at different altitudes are described in detail in the CFHT and VLT web sites and also listed in Table 2 of Coustenis et al. (2005a). These authors have studied Titan with surface filters (the ones including contribution from the surface and centered in the methane windows at 1.08, 1.09, 1.28, 1.6 and 2.0 micron) showing bright and dark features on both hemispheres. The atmospheric filters probe different altitude levels and are centered in the methane bands (at 1.04, 1.24, 1.64, 1.75, 2.12 and 2.17 micron - see Table 2 with altitude range and description of filter widths). Some filters contain both surface and atmosphere contributions (NB_1.04, NB_1.08, NB_1.28, H1, PaBeta, J1, Hcont, IB_2.00), yet we will consider mainly atmosphere-probing ones in this paper.

Send offprint requests to: M. Hirtzig

Table 1. Titan adaptive optics observations from 1998 to 2005 with CFHT/PUEO and VLT/NACO.

Date (UT)	Inst.	Filters	Solar phase angle	SEP LCM	Seeing
26 Oct 1998	PUEO	J1, J2, H1, H2	+0.51°	93-97°	
07 Mar 2001	PUEO	J2, J1, Jcont, H1, Hcont, Kcont	+5.83°	85-87°	0.8-1.0
08 Mar 2001	PUEO	I, PaGam, HeI, H1, Hcont, FeII	+5.80°	108-110°	1.0-1.2
04 Dec 2001	PUEO	H1, FeII, Jcont, J1, J2, HeI, PaGam, K, K', H2(1-0)	+0.29°	112-119°	0.5-0.8
13 Nov 2002	PUEO	BrGam, H2(1-0), FeII, H2, J2, J1, H1	-3.78°	283-287°	0.6-0.8
14 Nov 2002	PUEO	J1, J2, H1, H2, FeII, BrGam, H2(1-0)	-3.68°	305-309°	0.3-0.8
20 Nov 2002	NACO	NB_1.08, NB_1.24, NB_1.28, NB_1.64, NB_1.75, NB_2.12, NB_2.17	-3.13°	81-82°	1.7-2.3
20 Nov 2002	PUEO	J1, J2, H1, H2, FeII, BrGam, H2(1-0)	-3.11°	83-85°	0.7-1.0
21 Nov 2002	PUEO	J1, J2, H1, H2, FeII, BrGam, H2(1-0)	-3.00°	103-107°	0.5-0.8
25 Nov 2002	NACO	NB_1.08, NB_1.09, NB_1.24, NB_1.28, NB_2.12, NB_2.17	-2.60°	189-191°	1.3-1.6
26 Nov 2002	NACO	NB_1.08, NB_1.24, NB_1.28, NB_1.64, NB_1.75, NB_2.12, NB_2.17	-2.49°	211-214°	0.9-1.0
07 Jan 2004	PUEO	FeII, H2(1-0), H2, H1, PaBeta, J2	+0.80°	11-13°	0.7-1.0
08 Jan 2004	PUEO	H2(1-0), BrGam, K, K', J1, J2, J, PaBeta, Jcont	+0.91°	31-34°	0.4-0.6
25 Apr 2004	NACO	IB_2.00, NB_2.12, IB_2.15, NB_2.17	+5.65°	344-346°	0.5-0.6
16 Jan 2005	NACO	NB_1.28, IB_2.00, NB_2.12, IB_2.15, NB_2.17	+0.24°	192-194°	0.4-0.7

1.1. Observations

The data we analyze here refer to observations of the Titan atmosphere as listed in Table 2. We added up our images taken on the same day in a given filter to recover the best SNR possible. The NACO dates correspond to Titan angular radii of 0.44 for 2002 and 2005, and 0.37 for 2004 respectively. The PUEO data correspond to apparent radii of 0.37, 0.43 and 0.44 for 2001, 2002 and 2004 respectively. This explains the variations in Titan's apparent size in the figures herein, as in Fig. 1 for instance, even if Titan is observed with the same instrument. As listed on the logbook (Table 1) NACO images suffered occasionally from poor seeing conditions. Indeed the seeing was around 2 arcsec in 2002, with the optimal conditions (around 1 arcsec) on the last night. In 2004, the seeing was better, but the wind was too strong to allow us to acquire many images. Nevertheless, the few we managed to harvest afford a good seeing of around 0.6 arcsec. Finally, the 2005 NACO images did benefit from a good (0.4-0.6 arcsec) seeing. In comparison, all PUEO images prior to 2004 were taken with a good and stable seeing conditions, around 0.6 arcsec during all our observational runs, even reaching sometimes 0.4 (on the 14th Nov 2002).

In January 2004, we faced a serious problem with PUEO/KIR, because the telescope seemed to drift under its own weight. This drift caused our images to be somehow blurred and the later the time of observation (i.e. the closer Titan was to the horizon), the worse the drift. To be more specific, images acquired before 13UT did not show a detectable drift, and those taken after 15UT showed nearly a 2-arcsec drift. For the final processing step, namely deconvolution, this was a problem to be tackled : theoretically, PSF and Titan images are supposed to be acquired at short time intervals to ensure that the observing conditions are the same, and usually the PSF taken in the same filter and not long before or after the Titan image is the logical choice. But this was not always possible, and we sometimes had to choose another PSF instead of the "ideal" one. Usually this happened when the PSF could not be acquired at all or proved to be corrupted (low S/N ratio, inadequate drift representation of the Titan image, etc). In the case of the drifted 2004 PUEO images the drift of the telescope was the critical parameter, because it varied rapidly, growing by 1 arcsec in one hour at the end of the night. Thus we had to test all PSFs acquired during the night in order to find the one that would reduce or hopefully correct the Titan drift. Otherwise, a PSF with a drift bigger than the Titan image one would compress Titan's disk into an unphysical oval shape; on the other hand, a PSF not drifted enough would not correct Titan's drift. Finally, we trust our 2004 PUEO images only when several of them show the same result whatever the deconvolution method and they are consistent from one filter to another.

1.2. Data processing

A processing similar to that described in Combes et al. (1997), Coustenis et al. (2001) and Coustenis et al. (2005a) was applied to all our images, namely the regular flatfield and bad pixel correction, followed by deconvolution using standard photometric stars as PSF references. This returned diffraction-limited images in most cases where we used the Magain deconvolution, yet we had to sometimes choose lower resolution deconvolution methods (Bratsolis' version of the Lucy-Richardson method) for cases of extremely poor seeing (for Oct 1998, Mar 2001 and Jan 2004 PUEO images, in particular). We took great care to use only one method for a given series of observations, so as to ensure that comparisons within one night are still valid and suffer mainly from systematic errors (which are not a problem when we discuss *relative* measurements). Exceptions are the 1998 and January 04 PUEO series which we deconvolved with the Bratsolis RL method. See section 3.1 of Coustenis et al. (2005a) for more details on the deconvolution processes.

Note that we chose for this study not to correct for center-to-limb effects, contrary to Coustenis et al. (2005a). Since we focus here only on the study of Titan's limb (or a one-resolution-element-thick ring on Titan's limb), the center-to-limb effects

Table 2. N/S ratio characterizing the North-South Asymmetry from 1998 to 2005. We also show the altitudes probed at the limb by the different filters used.

Filter	Wavelength (μm)	Alt limb mini(km)	maxi(km)	N/S ratio 1998	2001	2002	2004	2005
NB_1.04	1.040 ± 0,007	36	47	-	-	1.019±0.005	-	-
NB_1.09	1,094 ± 0,0075	46	58	-	-	0.987±0.004	-	-
PaGamma	1,094 ± 0,005	50	58	-	0.872±0.015	-	-	-
J2	1,181 ± 0,064	81	205	0.883±0.089	0.964±0.016	1.162±0.021	1.132±0.045	-
Jcont	1,207 ± 0,007	70	88	-	0.877±0.018	-	1.043±0.048	-
NB_1.24	1,237 ± 0,0075	46	60	-	-	0.974±0.011	-	-
NB_1.28	1,282 ± 0,007	16	17	-	-	-	-	-
PaBeta	1,282 ± 0,007	16	17	-	-	-	-	-
J1	1,293 ± 0,070	12	104	-	-	-	-	-
Hcont	1,570 ± 0,010	8	9	-	-	-	-	-
H1	1,600 ± 0,080	8	125	-	-	1.027±0.021	0.864±0.042	-
NB_1.64	1,644 ± 0,009	45	322	-	-	1.549±0.015	-	-
H2	1,640 ± 0,050	21	322	0.812±0.094	-	1.102±0.009	0.927±0.049	-
FeII	1,644 ± 0,007	45	280	-	1.326±0.048	1.600±0.032	1.545±0.084	-
NB_1.75	1.748 ± 0,013	47	318	-	-	1.091±0.012	-	-
IB_2.00	2,000 ± 0,030	9	201	-	-	-	1.111±0.036	1.328±0.012
NB_2.12	2,120 ± 0,010	17	20	-	-	0.623±0.008	1.068±0.034	1.216±0.023
H2 (1-0)	2,122 ± 0,010	17	24	-	0.683±0.028	0.665±0.038	1.021±0.055	-
IB_2.15	2.150 ± 0,030	19	214	-	-	-	1.160±0.013	1.350±0.012
BrGamma	2.166 ± 0,010	40	311	-	-	1.333±0.034	1.453±0.122	-
NB_2.17	2.166 ± 0,010	40	311	-	-	1.091±0.012	1.357±0.036	1.653±0.027

are indeed more significant than in the study of the center of Titan's disk (Coustenis et al. (2005a)) The correction is far more sensitive to the application of a cylindrical filter (definition of the disk's radius and center) near the limb than in the center. If a cylindrical mask is shifted by even only one pixel from the real position of Titan's disk center, then the flux variation on the limb can easily reach 40%. The same occurs if the cylindrical mask radius is one pixel larger or smaller than Titan's real radius. All this would lead to unnecessary errors, and since we will only consider relative comparisons hereafter, we did not correct for center-to-limb effects, studying only a one-resolution-element-thick torus of pixels on the disk limb (from about 70 to 90° from the nadir).

1.3. Radiative transfer model

Alberto?? The efficient study of atmospheric images requires a complete radiative transfer model to recover altitude information for each filter used. Herein we use the microphysical and radiative transfer code of Rannou et al. (2003), which is an updated version of the one described in McKay et al. (1989). This model assumes that aerosols in Titan's atmosphere are fractal-shaped (Rannou et al. (1995)). The haze profile and all the parameters for this model are fully described in Rannou et al. (2003), however in Coustenis et al. (2005a) and the work herein we used the updated parameter values proposed by Negrão et al. (2004), whose work is based on ISO near-infrared measurements (from 2.5 to 5 micron). The alterations, comparing with Rannou et al. (2003), consist in an overall increase of the haze density on its vertical profile, calculated by the microphysical part of the model, by 40%. Also, although the altitude of the haze cut-off needed remains the same as the one used in Rannou et al. (2003), the shape of the haze vertical profile below the cut-off is slightly different. A new methane abundance near the surface of 3-4% instead of 8%, consistent with recent DISR observations (Bézard et al. (2004)), was used in these calculations. The methane absorption coefficients used in this model are taken from a re-analysis of K. Strong and L. Giver data by R. Moreno as explained in Coustenis et al. (1995) and references therein for the 1.08 and 1.28 micron windows, and from the Hilico et al. (1994) updated database at and beyond 1.6 micron. For an update on this model and recent results, see Coustenis et al. (2005b).

This model can return three altitude calculations per filter depending on the phase angle considered (here we study only the limb, 80° away from the nadir) : the nominal one (used only in Section 4) corresponds to the average $\tau_{eff} = 1$ level over the bandwidth of the filter, translating into the lowest level probed by photons, this opacity parameter taking into account forward- and backscattering by the atmosphere particles. These particles may have slightly different behaviors depending on the wavelength and the fast variation of methane absorption coefficients within a methane window: thus we chose to consider the minimum and maximum $\tau_{eff} = 1$ layers over the FWHM of the filter, as reported in Table 2. Such values give a good thickness estimate of the layer probed. Note that a narrow-band filter will not necessarily probe a very specific layer if it covers a region where methane coefficients vary quickly (see for instance the NB_2.17 and NB_1.24 NACO filters, probing respectively the 40-300

and 46-50km ranges: though with a similar FWHM, the former spans a larger altitude range because it overlays high methane coefficient variations).

2. Evolution of the North-South asymmetry on Titan

Many features appear on the limb of Titan. Some images probing the atmosphere (see Table 2) show the well-known for the past 10 years bright South Pole of Titan. However, since 2001 we observe in some of these filters (at 1.64, 1.75, 2.17 micron) an inversion of the North-South Asymmetry with a currently bright north pole (some evidence for a NSA inversion in the visible existed previously, as described in Lorenz et al. (1999)). This is an expected (by the seasonal models) return to the Voyager situation, where the South limb was bright in the visible, but dark in the IR, anti-mirrorring the Northern limb. This situation had reversed in the 90's, showing the famous "Titan's smile" on each AO and HST image (see for instance Saint-Pé et al. (1993) and Caldwell et al. (1992) respectively). In some cases, as at 1.04, 1.09 and 1.24 micron, we find currently components of both tendencies to be present. In Figs. 1 and 2, we illustrate the NSA evolution as a function of altitude probed by different filters. We quantify the North-South contrast by computing the ratio of the N intensity over the S one, as reported in Table 2. Error bars rise mainly from the variation of intensity on the limb from one resolution element to another. For this study, we only considered "uniform" and feature-free limbs to avoid deconvolution artefacts (the ringing effect is present, but we did not try to correct it with a mere center-to-limb effect compensation with perhaps dubious results). In particular, the case of the 2.12 micron filter is used only as a confirmation and not as a detection of NSA variations : as we will describe in subsection 4.2, the Southern limb on the 2.12 micron images is not uniform and continuous, showing many features that cannot be sensibly eliminated to compute a true average intensity for the S limb.

In Figs. 1 and 2, we find that there is a certain evolution with time : the Titan "smile" has faded in most of the images and the north pole appears brighter than the southern one in more and more filters as time goes by. Our study indicates that this evolution is a function of the altitude levels probed and that the NSA reverses propagating to lower altitudes with time. Starting out at higher levels in the atmosphere, the bright northern pole replaces the southern one, as with time the reversal affects lower altitudes.

- **Variations as a function of time :** It is clearly visible in Figs. 1 and 2a that a given filter showing the NSA witnesses its reversal with larger and larger N/S ratio values as time goes by; for instance, the PUEO J2 filter shows such a trend from 1998 till 2005 (within error bars, the NSA seems not to evolve between 2002 and 2004[1]. In 2002, the famous "Titan smile" is but a memory ! In 2004, all images even show a bright northern limb.
- **Variations as a function of altitude :** Figs. 1 and 2b also confirm that the NSA evolves differently depending on the altitude probed. For instance, in 2001, the PaGamma filter (at 1.094 micron, probing the troposphere) showed a bright South pole (N/S=0.87), which appeared negligibly dim above the tropopause (Jcont - 1.207 micron : N/S=0.88) and fading in the upper stratosphere (J2 - 1.181 micron : N/S=0.96). Three years later, the NSA has reversed, but it is more pronounced at higher altitudes (J2 : N/S=1.16) than deeper in the troposphere (NB_1.04 : N/S=1.019). The same applies for all the filters covering the same methane window (H2(1-0) - 2.12 micron - and BrGamma - 2.17 micron - in the K band, for instance). This underlines the slow motion and high inertia **(Pascal, Sebastien: peut-on quantifier cette inertie?)** of the whole atmosphere : deeper layers respond more slowly to the change of solar insulation, as predicted by the models.
- **Variations as a function of wavelength :** N/S ratios seem to also vary as a function of wavelength. In 2002, the NSA is definitely reversing (2.12 micron measurements are not counter-examples), yet in Table 2 the N/S values are more contrasted at longer wavelengths than at 1 micron. In the J band, the N/S contrast varies by about ±0.2 (translating into variations in intensity of about ±20%), while it can reach 40 to 60% in the K and H bands ! It then seems that the tholins and aerosols are less involved in the NSA migration than methane particles, since tholins still blur the signal all over Titan's disk when they are detectable (that is below 1 micron). This is logical, because larger particles (such as tholins and aerosols) are less sensitive to the atmospheric currents induced by the change of solar insulation, while light particles are easily swept away to the winter hemisphere. **(Pascal : ca te semble véridique? si oui, peut-on quantifier cette taille de grains d'après le peu d'infos qu'on a?)**

3. Phase and diurnal effects on Titan

The images taken in the atmospheric filters that we use contain a number of bright features. Some of them have to do with solar phase effects, as can be seen on the Western limb of Titan (to the left) in 2002 images (Fig. 1). The brightness here is due to the 2.5 degree phase effect. In Tables 1 and 3 are given the numerical values of the solar phase angle : if it is positive, then the solar phase effect is expected to appear on the Eastern limb (this evening limb is on the right of all our North-up oriented images).

---

[1] In 2004, we suffered from mechanical problems, rendering the analysis PUEO 2004 data difficult; furthermore, all 2.12 micron images could not be used in this study (as explained hereabove), diminishing the number of data points to be drawn. Along with legibility, these are all the more reasons for us to show only the J band data in Fig 2b.

Table 3. E/W ratio characterizing the solar phase effect, at various altitudes. Only relevant data are given here (surface images are not used). Some results are given in bold face (unexpected values indicative of a "morning fog" effect) or in italic (insecure values because error bars can change the interpretation) : see text for details.

Filter	Alt limb mini-maxi (km)	E/W ratio						
		Oct 98 (+0.5°)	Mar 01 (+5.8°)	Dec 01 (+0.3°)	Nov 02 (-3°)	Jan 04 (+0.8°)	Apr 04 (+5.6°)	Jan 05 (+0.2°)
NB_1.04	36- 47	-	-	-	0.907±0.011	-	-	-
PaGamma	50- 58	-	-	*1.032±0.036*	-	-	-	-
J2	81-205	**0.897±0.050**	1.131±0.054	**0.976±0.023**	0.878±0.046	*1.008±0.084*	-	
Jcont	70- 88	-	1.049±0.023	*0.982±0.035*	-	1.101±0.044	-	-
NB_1.24	46- 60	-	-	-	0.854±0.006	-	-	-
NB_1.64	45-322	-	-	-	0.839±0.093	-	-	-
H2	21-322	*0.970±0.082*	-	-	0.880±0.033	*1.000±0.349*	-	-
FeII	45-280	-	-	**0.906±0.084**	0.851±0.058	*1.066±0.146*	-	-
NB_1.75	47-318	-	-	-	0.876±0.009	-	-	-
NB_2.12	17- 20	-	-	-	0.920±0.013	-	1.328±0.060	**0.964±0.023**
H2 (1-0)	17- 24	-	-	*1.066±0.134*	0.868±0.061	**0.923±0.067**	-	-
IB_2.15	19-214	-	-	-	-	-	1.093±0.061	**0.940±0.044**
BrGamma	40-311	-	-	-	0.932±0.050	*1.033±0.140*	-	-
NB_2.17	40-311	-	-	-	0.876±0.009	-	1.329±0.111	**0.815±0.037**

When we find in such conditions a brighter morning (i.e. West, on the left) limb, we interpret this as a "morning fog" effect (according to the description first made in Coustenis et al., 2001).

Table 3 summarizes all the measurements of the E/W contrast in atmosphere-probing images. Error bars originate in the flux variations within three consecutive resolution elements on each limb, exactly as was described for the N/S ratios. Unexpected E/W values (i.e. when the brightness is not on the limb where it should appear given the sign of the solar phase angle) are shown in bold face style. On the other hand, insecure values are given in italic (i.e. if 1.0 is a solution, meaning that there is no way to tell which side is the brightest).

When the phase angle is large (e.g. Mar 2001 (+5.8°), Nov 2002 (about -3°) and Apr 2004 (+5.6°)), then the phase effect is obvious, with a 10-15% contrast between the Eastern and Western limbs, the brightness always on the expected side (respectively E, W and E).

In October 1998, December 2001, January 2004 and January 2005, the phase angle of our observation is small and in some filters we do not easily detect the phase effect on the evening side; many of the contrast values are close to 1 within 10% of uncertainty. Narrow band filters show that within error bars, the E and W limb fluxes are similar (many "insecure results" in Dec 01 and Jan 04 are in italic, underlining that the error bars are large enough to allow for a "phase-effect" solution). Yet in several cases (J2 and H2 in Oct 1998, J2 and FeII in Dec 2001, H2(1-0) in Jan 2004 and all NACO images in Jan 2005) error bars cannot account for the unusual aspect of the disk : the phase effect would have appeared faintly on the Eastern limb (to the right) but the Western limb is about 3-19% brighter. With low positive values of the solar phase angle (+0.2 to +0.5°), the detection of such a brightness on the morning side could be attributed to a "morning fog" phenomenon (the 1998 PUEO data allowed for such an interpretation in Coustenis et al. (2001)).

It would seem that we have some evidence, on dates where it is possible (Oct 1998, Mar 2001, Jan 2004 and Jan 2005, with 7 firm detections and 8 tentative ones over the total of 16 images), of a bright morning limb which would tend to corroborate findings by Coustenis et al. (2001) on an enhancement of condensates during the Titan night (8 Earth days, though the super-rotation of Titan's atmosphere would lead to shorter nights for stratospheric clouds), manifesting itself in a "morning fog" phenomenon at stratospheric altitudes. Indeed, most of the images showing this phenomenon are probing the stratosphere mainly. Exceptions are the 2.12 micron filters, which probe mainly the troposphere. We cannot infer whether the detection corresponds to a faint nightly condensation occurring at these altitudes, or if it is a contribution of the larger phenomena in the stratosphere detected by the 2.12 micron photons when they cross these layers before reaching the $\tau_{eff} = 1$ level.

This detection has also been confirmed by other teams with the HST in the 2000's (Young, private comm.) or the Keck in 2005 (de Pater, private comm.). What we find is that the fainter the solar phase effect, the easier the detection of the "morning fog": in January 2004 (phase +0.8°), we have a definite 8% effect measurement, but all other images are insecure, furthermore one image (Jcont) does show a regular phase effect. In December 2001 and October 1998 (phases +0.3 and +0.5° respectively), we detect a 10% effect at most, with 3 detections and 4 undefinite answers (but no regular phase effect). Finally, in January 2005 (phase +0.2°), a 18% "morning fog" effect is detected, on all 3 images.

Table 4. Observations of the southern polar feature (SPF)

Instrument	Date/time (UT)	Filter	Coordinates of S	Contrast
PUEO	05 Dec 2001/07:24	J1	79±9 S, 157±122 W	
PUEO	05 Dec 2001/08:49	PaGamma	84±12 S, 160±150 W	
PUEO	05 Dec 2001/12:26	H2(1-0)	84±7 S, 165±101 W	
PUEO	05 Dec 2001/12:26	H2(1-0)	82±6 S, 156±70 W	
PUEO	05 Dec 2001/12:26	H2(1-0)	73±14 S, 256±70 W	
PUEO	05 Dec 2001/13:01	K'	81±8 S, 225±69 W	
PUEO	05 Dec 2001/13:01	K'	84±6 S, 147±140W	
PUEO	13 Nov 2002/13:20	H2(1-0)	81±9 S, 337±135 W	
PUEO	13 Nov 2002/14:23	H2	87±13 S, 308±90 W	
PUEO	13 Nov 2002/14:23	H2	78±35 S, 304±56 W	
PUEO	13 Nov 2002/15:29	H1	84±13 S, 54±50 W	
PUEO	13 Nov 2002/15:29	H1	76±7 S, 302+/45 W	
PUEO	13 Nov 2002/15:58	H2(1-0)	83±7 S, 315±135 W	
PUEO	14 Nov 2002/13:24	H2(1-0)	88±9 S, 243±116 W	
PUEO	14 Nov 2002/15:04	H1	86±12 S, 282±77 W	
PUEO	14 Nov 2002/15:24	H2(1-0)	86±10 S, 282±102 W	
NACO	20 Nov 2002/09:05	2.12	80±4 S, 260±27W	
PUEO	20 Nov 2002/12:22	H1	71±13 S, 249+/45 W	
PUEO	20 Nov 2002/13:14	H2(1-0)	83±9 S, 237±123 W	
PUEO	20 Nov 2002/15:37	H2(1-0)	81±8 S, 228±80 W	
PUEO	21 Nov 2002/12:08	H2(1-0)	70±9 S, 209±27 W	
PUEO	21 Nov 2002/14:03	H2(1-0)	72±11 S, 223±30 W	
NACO	25 Nov 2002/07:51	2.12	84±4 S, 312±42 W	
NACO	26 Nov 2002/07:48	2.12	84±5 S, 327±39 W	
PUEO	07 Jan 2004/12:36	H2(1-0)	84±6 S, 112±110 W	
PUEO	08 Jan 2004/10:40	H2(1-0)	80±10 S, 185±56 W	
PUEO	08 Jan 2004/11:29	H2(1-0)	85±14 S, 209±151 W	
PUEO	08 Jan 2004/12:53	H2(1-0)	NA	
NACO	25 Apr 2004/22:50	2.12	85±9 S, 185±46 W	
NACO	25 Apr 2004/23:20	2.00	88±4 S, 78±79 W	
NACO	26 Apr 2004/00:07	2.12	82±7 S, 150±30 W	
NACO	26 Apr 2004/00:15	2.15	81±7 S, 140±36 W	
NACO	16 Jan 2005/03:58	2.12	81±6 S, 355±90 W	

4. A southern bright revolving feature

Besides these features, we have observed other discreet bright areas near Titan's south pole (sometimes on top of a fine bright south pole limb) in filters indicating that we are looking at the atmosphere *at the limb* (such as at 1.04, 1.24 and 2.12 micron). This feature has been oberved since 2001 in different filters (Fig. 5) and by different teams. Note the absence (or very rare presence) of bright features in the North, apart from the bright Northern limb certainly due to the NSA (the North Pole cannot be seen in most of our data, except in 1998). It is particularly visible in 2.12 micron images, where the Southern limb appears after deconvolution as a group of three features: the SPF is bracketed by two elongated features, on the East and West sides. We will call them from now on EPF and WPF respectively.

4.1. Description of the Southern Polar Feature

Now we concentrate on SPF (around and very near Titan's south pole, in the 2.12 micron images). We had noticed and presented this phenomenon in 2002 (Coustenis et al. (2002), Coustenis et al. (2003), Gendron et al. (2004)). All our SPF detections are summarized in Table 4 and Fig. 5. This feature is also observed clearly at least in the Keck and Gemini images taken

– around 2.5 micron: with a broad-band filter (K', 1 micron wide), on December 10 and 11, 2001 (Brown et al., 2002);
– around 2 micron : with a broad-band filter (also K', but 0.3 micron wide), on July 27-August 1, and 7-14 October 1998 (Gibbard et al., 2003);
– around 2-2.25 micron with narrow-band filters (H2(1-0), NB2108) on 9, 18, 20 and 21 December 2001 (Roe et al., 2002).

It was interpreted as one of the many transient methane clouds observed by these teams. It has also beeen observed by Cassini at T0 and TA on 3 July and 26 October 2004. Finally, a brief study was presented by Schaller et al. (2004) regarding the luminosity variation of the South Polar Feature (SPF) within one year with a low-resolution telescope.

Our own images show this feature clearly in certain filters (Table 4). The size of this feature seems to vary as a function of its position with respect to the observer's. In any case, this feature does not seem to grow or flatten as a function of time within our resolution. Only its brightness seems to change, but we can correlate this more often than not with the appearance of the NSA : the brighter the Southern limb, the brighter the SPF within it. Its average size corresponds to 2x1 elements of resolution for PUEO observations (pixel angular dimension is 0.0348 arcsec in this case) and to 3x1.5 for NAOS (pixel size is 0.01326 arcsec). This leads to an angular size of about 0.09x0.05 arcsec (±0.01) (according to Shannon's principle, the size of one resolution element must be twice the nominal angular size of the detector's pixels) This pertains to a projected surface reaching 700x3,000 km, i.e. 4-5% of cloud cover (with respect only to the sunlit half of the satellite that we can see at a time).

We hereafter study the nature of this phenomenon observed in Titan's atmospheric images in view of the recent announcements of the detection of "clouds" over Titan's south pole.

4.1.1. Speed of the SPF

Within one night of observation (we acquired several 2.12 images the same night for nearly all our 2002 and 2004 runs), the SPF often seems to be unmoving within our error bars. From one night to another, we detect a motion from which we compute to be a 3 m/s velocity. This value is compatible with all wind speed values reported from observations (0.5 ± 3 m/s by VIMS -Momary et al. (2004)- 34 ± 13 m/s at most in the upper troposphere by ISS -Porco et al. (2005)) and models (Hourdin et al. (1995, Tokano et al. (2001), Rannou et al. (2004)). With this mere velocity computation we could assume that the SPF lies in the lower troposphere, or perhaps in the upper troposphere if we suppose that it is only faintly driven by the average winds, allowing it to move more slowly than the usual winds (but in the same direction anyway).

Yet in some cases the apparent speed can reach about 120 m/s ! (167_{-96}^{+230}m/s from the positions measured on the 13 Nov 2002 H2 and H1 images ; a similar case occurs in the measurements on the 25 Apr 2004 IB_2.00 and NB_2.12 images returning a 122_{-49}^{+81}m/s velocity). We cannot put faith in such high speed motions for a feature detected only by troposphere-probing filters : such values correspond to upper stratosphere winds (stratospheric winds reach at least 75m/s at 200km -Luz et al. (2005)-, up to 210m/s -Kostiuk et al. (2001)-). A joint operation between the JPL, the JIVE/VLBI and Cassini-Huygens/DWE teams measured prograde wind speeds of about 120m/s at 120km -*http://www.esa.int/SPECIALS/Cassini-Huygens/SEMA8SXEM4E_0.html*. Furthermore we cannot explain why the trajectory of the SPF would be so erratic. A rather plausible explanation can be found if one considers that the computation of the speed assumes that the bright features seen on the images correspond to the same physical object; were this not the case, an answer to this dilemma could be given by Earth meteorologists, and is explicitly confirmed by VIMS **(Brown et al ?)** and ISS (Porco et al. (2005)) observations at T0 and TA : the feature looks like a large ring of thin clouds or haze, deforming, with little bright clouds trapped within it, appearing and disappearing randomly, recently desintegrating, something we cannot resolve with Earth-based AO systems.

4.1.2. Altitude of the SPF

The detection of the SPF mainly occurs at 2.12 micron in our images (at 2.108 micron in Bouchez (2003) Palomar observations). We have some hints that it is decipherable in other broad-band filters (J1, K', H2 or H1 in particular), but such filters cover large spans of altitude within Titan's atmosphere, giving little indication as to the exact position of the SPF. Since 2002, we have been adding other narrow-band filters to our filter wheels to better restrain the SPF altitude. We had noticed that even though the SPF was bright and obvious at 2.12 micron, it was nowhere to be seen on 2.17 images.

We will consider here for instance 2004 NACO data (some of which were published in Gendron et al. (2004)), presented in Fig. 6. In the 2.00 micron image, for instance, we note the presence of the SPF nearly atop the South Pole (lat=85 south ±3°, long=110 W ±20°). The surface contribution in this filter is predominant, but on the limb, we can probe down to the low troposphere (9 km). The SPF is particularly visible in 2.12 micron images, where it is bracketed by the EPF and WPF features. At 2.15 micron, the three features are still visible, but the SPF is fading, and the WPF seems to be the brightest one. Finally, the central southern feature (SPF) and the two adjacent ones (EPF and WPF) have disappeared in images taken at 2.17 micron (Gendron et al., 2004).

According to our altitude estimates, the 2.17 micron filter probes levels in the highest atmospheric regions. EPF, WPF and SPF are not visible above 80 km. We probe deeper with 1.15, where EPF and WPF appear (with WPF slightly brighter than EPF due to the phase effect), then deeper down SPF appears. Further down only SPF remains, very intense (EPF and WPF are still there, detectable, but less contrasted with respect to SPF). We conclude that EPF, WPF and SPF are atmospheric phenomena (since they do not show up in images of Titan's surface alone) which are located at different atmospheric levels (we assume here the change in luminosity is due to both altitude and phase effects and not to spectral features).

For statistical purpose, we will now consider all our observations as a whole. We note that :

– At 2.00 and 2.12 micron (IB_2.00, H2(1-0) and NB_2.12), the SPF is clearly visible, along with its two EPF and WPF companions. The narrower filters probe down to 17-20 km (nominal value : 18 km), meaning that the SPF is certainly between this limit and the observer.

- On the NB_1.04, PaGamma (1.09 micron) and IB_2.15 filters, the SPF is not always clearly visible, fading into the background along with both the EPF and WPF features. Depending on the observation we want to believe in, the SPF might be above 20 (IB_2.15, nominal : 50 km), 36 (NB_1.04, nominal :42 km) or 50 km (PaGamma, nominal :53 km).
- At 2.17 micron (NB_2.17, BrGamma) the SPF is not visible anymore, and EPF and WPF merge into the southern limb. This means that in the 40-311 km range probed by these filters, there is no hint of the SPF. The preferential altitude probed here is about 83 km.

As a conclusion, from the nominal values of the altitudes probed by these different filters, the SPF must be located between 18 and 83 km, with a higher probability between 17 and 40 km (if it is a condensation cloud). In any case, this constrains it between the surface and the low stratosphere, below 80 km of altitude. In January 2005, we acquired new data resolving the K band with a Fabry-Pérot experiment at the VLT (FPI mode of NACO), reaching a 2 nm wavelength resolution, which will constrain more efficiently this altitude computation.

4.2. The case of the EPF and WPF companions

On all images, the S feature is paired with two unmoving companions on each side on the limb. They are neither moving nor changing in shape, yet one is always longer than the other, more precisely the one on the solar-illuminated side is usually longer (for instance, on the 2002 2.12 micron image in Fig. 1, the solar phase effect is on the western limb, and the W companion is spanning further on the limb). We cannot believe that there is such a gap between the bright SPF and these two companions, because it is only one resolution-element wide (and the Shannon principle requires it to be at least twice larger to be physically valid).

Many atmospheric models (Rannou et al. (2002), Rannou et al. (2004) for instance) foresee two stratospheric hoods of haze swept away from the Equator by the atmosphere dynamics. We believe that the two companions are but a deformed appearance of such a hood : there is evidence for a strange serpentine feature above the 60th parallel, also described as an "equatorial cirrus" (Roe et al. (2002a)) that might represent the upper limit of this hood. We can therefore guess that this hood is brighter on the solar-enlightened limb, and is uniformly englobing the South Pole southward from the 60th parallel. Within this hood lies the SPF. After deconvolution, the hood is completely deformed : the ringing effect only enhances the portion of the hood overlapping the disk's limb, and there is only a little indication of its north extent, near the southern third of the disk. Furthermore, a gap is created by the deconvolution around the SPF, darkening artificially the limb and creating this "two companions" appearance. This led us to omit all the 2.12 images for the NSA evolution quantification, because there are too many artefacts mixing with each other to ensure a correct reading of the intensity of the Southern limb.

4.3. Investigating the nature of the SPF

The SPF has been currently observed many times from the ground and space, including Cassini. Its very motion is incompatible with a surface-connected feature, even though it might be some orographic cloud or another surface-related phenomenon, mayhaps cryovolcanism-induced plumes.

Earthling eyes would tend to assimilate the SPF to a polar aurora, like the ones seen on Earth, or even on Jupiter (Waite et al. (2000)) and Saturn (Clarke et al. (2005)). The aurora is by definition the locus of interaction between solar wind particles trapped in the magnetosphere and the ionosphere particles. Yet Titan owns no detectable magnetic field, and borrowing field lined from Saturn's magnetosheat would lead to very peculiar magnetospheric phenomena. First, the interaction would vary with respect to Titan's orbit, with a period similar to the one of the satellite's revolution. Moreover, the penetration of Titan into Saturn's magnetosheat will deform the field lines like a shell, compressing them in particular above Titan's trailing hemisphere (Neubauer et al. (1984), Blanc et al. (2002)). Such a configuration would lead to aurora-like phenomena uniformly distributed over Titan's disk, which is not at all what we see here. The small size of our sample might induce observationnal errors, but this seems unlikely, since Cassini (e.g. ISS and VIMS) detected clearly the SPF above the South Pole, as expected. The motion of these clouds resolved by ISS resembles cumulus convection (Porco et al. (2005)) induced by the solar insolation on the summer pole. In any case, magnetosphere-driven particles might be involved in the apparition of the tracer we detect, as we will describe hereafter.

The crucial point of our investigation is the difference we make between the atmospheric phenomenon we look for and the SPF we detect : the SPF is but a mere tracer trapped into a larger atmospheric phenomena. This can explain why the SPF deforms so quickly from time to time : the first tracer disappears while another one is created at another place, still within the larger atmospheric system. We then have to describe both the tracer and the trap. The tracer itself is a very bright feature, probably a methane/ethane cloud or a thunderstorm, characterized by a short lifespan (about 2-3 days up to one week, if we believe that the largest speeds or widest motions detected correspond in fact to changes of the very appearance of the whole system). Its brightness (about 300% brighter than the surrounding areas) is either due to a high local concentration of reflective or retro-diffusing particles (aerosols ? dust ? methane/ethane snowflakes ?) or/and a large physical size of the tracer (CASSINI/ISS detected 100-km sized clouds around the South Pole). We can only guess its origin : if the "supersaturation of methane" hypothesis is confirmed,

then the creation of a cloud requires a large amount of CCN (cloud condensation nuclei) to account for the large lifespan of the cloud ; the creation of such CCN may involve cryovolcanism ejecting dust particles into the lower troposphere, solar wind excitation of upper atmosphere particles (both hypothesis still need further explanation as to the transportation of the CCN into the troposhere.), or aerosols brought from the upper stratosphere down into the troposphere by descending motions (as suggested by models: Hourdin et al. (2004), Rannou et al. (2004)).

The large phenomenon entrapping the SPF seems circular, as seen by Cassini, weakly centered on the South pole. Condensation above the summer pole is obtained in the General Circulation Model developed at the Institute Pierre-Simon Laplace for the atmosphere of Titan. While the dominant circulation pattern seen in the model is a large Hadley cell with ascending motions in the summer hemisphere and subsiding motions above the winter pole, a small stratospheric Hadley cell persists above the summer pole (see e.g. Fig.10 of Hourdin et al. (2004)). This cell may explain why enhancement of ethylene has been observed late in southern spring season (Roe et al. (2004)). It also keeps high aerosols concentrations in this region. Although clouds are not yet explicitly included in this GCM (work in progress), the subsiding motions that are present in the stratosphere right above the summer pole induce condensation of trace compounds such as ethane, acetylene and hydrogen cyanide, which can yield clouds in the upper troposphere, combined with the high densities of haze particles. In this 2-dimensional GCM, tropospheric zonal winds are not featuring a jet, but the meridional circulation seems to produce a small tropospheric cell above the pole which induces methane condensation in the 70-90 latitude range, consistent with the region where we detect the SPF, and with the Cassini images.

This hypothesis is still under investigations, and may need a confirmation with a full 3-dimensional model.

5. Conclusions and discussion

We have studied Titan's atmosphere with adaptive optics in the past 5 years and we report on results pertaining to atmospheric seasonal, diurnal and meteorological phenomena.

1. Titan's North-South asymmetry has reversed from the situation where in 1992 HST found the South Pole to be brighter than the Northern (Caldwell et al., 1992) in the near-infrared. This reversal is noted since 2001 in the data presented here (but was found to exist earlier from other studies in the visible). Our data show that this NSA reversal occurs first at higher altitudes (the ones more sensitive to insolation) and then propagates to lower levels. By 2004, the NSA is completely inverted at all wavelengths between 1 and 2 micron.

2. The diurnal effects ("morning fog") first described in Coustenis et al. (2001) are confirmed in our observations (in particular in 2005 VLT data). Phase effects appear on the limb closer to the Sub-Solar Point, as expected, with the corresponding limb up to 15% brighter than the opposite one in case of large (3°) solar phase angle. Other images, at low solar phase angles, with a faint phase effect on the evening side, allow us to detect a stronger diurnal effect on the morning terminator. (donner des indications sur les pourcentages et altitudes) We have made a statistically convincing case for the presence of such a phenomenon on Titan.

3. There is a large bright feature revolving around the south pole of Titan (mainly within the 80° parallel). Our data indicate that it is located between 17 and 83 km of altitude, more probably (if it is a condensation cloud) in the upper troposphere. We find from the footprints of our observations that the trajectory associated with the movement of this feature is erratic (most velocities indicate 3 m/s, but in some cases this speed is significantly higher), which is compatible with a fast deformation of the feature more than a real movement.

5.1. The NSA

The North-South Asymmetry (NSA) of Titan has been recorded since the Voyager encounters in the late 70's. At that time, Titan's season was just after vernal equinox, with the southern hemisphere brighter by about 20% than the northern in the visible (Smith et al., 1981; Smith et al., 1982: Letourneur and Coustenis 1993). This tendency reversed in 1990 in the blue (440 nm) and yellow (550 nm) wavelengths, with the northern hemisphere about 10% brighter than the southern (HST measurements by Caldwell et al., 1992). Indication of a further reversal since 1997, in the visible again, from HST images was found (Lorenz et al. (1999), Lorenz et al. (2001)), with the "smile" disappearing at 889 nm, although still visible at 953 nm and beyond.

These albedo changes are interpreted as seasonal variations (Sromovsky et al., 1981; Lockwood et al., 1986) related to the haze properties (such as the albedo increase of the haze particles with wavelength (McKay et al., 1989, Griffith et al., 1991)). As regards the temporal variations, it seems that the reversal settles in over a 5-year period, which is faster than the seven year period between equinox and solstice on Titan. Sromovsky et al. (1981) find a phase lag for the NSA of about 90 degrees relative to the solar.

Several mechanisms were proposed to explain the NSA (see Roos-Serote 2004 for a review), but a combination of compositional variations (Coustenis and Bézard, 1995; Bézard et al., 1995) and of dynamical effects seem to be the most plausible answer (Flasar et al., 1981).

Prior measurements indicated that during the Cassini/Huygens mission the NSA would be stable. From our data, and because we have altitude-discriminating information in our narrow-band filters, a more complicated pattern appears. We have followed the evolution of the NSA in the past decade, and more efficiently so in the past 5 years. We find it to be more pronounced at some wavelengths probing the higher atmosphere and to be slowly appearing in the lower levels and down to the troposphere at the current era.

Such information is crucial to the understanding of the atmosphere dynamics, and can be used to constrain current seasonal/photochemical/dynamical models, since it quantifies the spatial and temporal propagation of the NSA.

5.2. The "morning fog" effect

We find that our images show in a significant number of cases the presence of a bright morning limb when the phase effect is expected on the evening side. These cases were observed principally in filters probing atmospheric levels between 20 and 300 km (mainly the stratosphere, Table 3).

Microphysical models of Titan's haze (e.g. Rannou et al., 2003) predict the condensation of methane byproducts (such as ethane and acetylene as the most abundant ones) somewhere between 70 and 90 km of altitude (Coustenis et al., 2001). Thus, the observed morning/evening asymmetry that we find in our data since 1998 could be explained by a diurnal condensation cycle of the condensable species. Since on Titan one night lasts about 8 terrestrial days, even considering stratospheric winds of 100 m/s (Ref?), there is time enough for the condensation to occur during the low temperatures prevailing on the night side. This then manifests itself by a brighter cold morning limb with respect to the darker warmer evening side.

(Pascal: peut-on faire mieux avec les nouvelles measures et aussi avec nos connaissances actuelles sur les nuages, les temperatures, le methane, les vents, etc???)

5.3. Investigating the nature of the SPF

verif PhD Bouchez...

The SPF has been currently observed many times from the ground and space, including by Cassini. Its very motion is incompatible with a surface-connected feature, even though it might be some orographic cloud or another surface-related phenomenon, mayhaps cryovolcanism-induced plumes.

Earthling eyes would tend to assimilate the SPF to a polar aurora, like the ones seen on Earth, or even on Jupiter (Waite et al. (2000)) and Saturn (Clarke et al. (2005)). The aurora is by definition the locus of interaction between solar wind particles trapped in the magnetosphere and the ionosphere particles. Yet Titan owns no detectable magnetic field **(Pierre: ref ???)**, and borrowing field lines from Saturn's magnetosheat would lead to very peculiar magnetospheric phenomena. First, the interaction would vary with respect to Titan's orbit, with a period similar to the one of the satellite's revolution. Moreover, the penetration of Titan into Saturn's magnetosheat will deform the field lines like a shell, compressing them in particular above Titan's trailing hemisphere (Neubauer et al. (1984), Blanc et al. (2002)). Such a configuration would lead to aurora-like phenomena uniformly distributed over Titan's disk, which is not at all what we see here. The small size of our sample might induce observationnal errors, but this seems unlikely, since Cassini (e.g. ISS and VIMS) detected clearly the SPF above the South Pole, as expected. The motion of these clouds resolved by ISS resembles cumulus convection (Porco et al. (2005)) induced by the solar insolation on the summer pole. In any case, magnetosphere-driven particles might be involved in the apparition of the tracer we detect, as we will describe hereafter.

The crucial point of our investigation is the difference we make between the atmospheric phenomenon we look for and the SPF we detect : the SPF is but a mere tracer trapped into a larger atmospheric phenomenon. This can explain why the SPF deforms so quickly from time to time : the first tracer disappears while another one is created at another place, still within the larger atmospheric system. We then have to describe both the tracer and the trap. The tracer itself is a very bright feature, probably a methane/ethane cloud or a thunderstorm, characterized by a short lifespan (about 2-3 days up to one week, if we believe that the largest speeds or widest motions detected correspond in fact to changes of the very appearance of the whole system). Its brightness (about 100 to 300% brighter than the surrounding areas) is either due to a high local concentration of reflective or retro-diffusing particles (aerosols ? dust ? methane/ethane snowflakes ?) or/and a large physical size of the tracer (CASSINI/ISS detected the SPF and reported it as 100-km sized clouds around the South Pole, Porco et al., 2005 **- à vérifier**). We can only guess its origin : if the "supersaturation of methane" hypothesis is confirmed, then the creation of a cloud requires a large amount of CCN (cloud condensation nuclei) to account for the large lifespan of the cloud ; the creation of such CCN may involve cryovolcanism ejecting dust particles into the lower troposphere, solar wind excitation of upper atmosphere particles (both hypothesis still need further explanation as to the transportation of the CCN into the troposhere.), or aerosols brought from the upper stratosphere down into the troposphere by descending motions (as suggested by models: Hourdin et al. (2004), Rannou et al. (2004)).

The large phenomenon entrapping the SPF seems circular, as seen by Cassini, weakly centered on the South pole. Condensation above the summer pole is obtained in the General Circulation Model developed at the Institute Pierre-Simon Laplace for the atmosphere of Titan. While the dominant circulation pattern seen in the model is a large Hadley cell with ascend-

ing motions in the summer hemisphere and subsiding motions above the winter pole, a small stratospheric Hadley cell persists above the summer pole (see e.g. Fig.10 of Hourdin et al. (2004)). This cell may explain why enhancement of ethylene has been observed late in southern spring season (Roe et al. (2004)). It also maintains high aerosol concentrations in this region. Although clouds are not yet explicitly included in this GCM (work in progress), the subsiding motions that are present in the stratosphere right above the summer pole induce condensation of trace compounds such as ethane, acetylene and hydrogen cyanide, which can yield clouds in the upper troposphere, combined with the high densities of haze particles. In this 2-dimensional GCM, tropospheric zonal winds are not featuring a jet, but the meridional circulation seems to produce a small tropospheric cell above the pole which induces methane condensation in the 70-90° latitude range, consistent with the region where we detect the SPF, and with the Cassini images.

This hypothesis is still under investigation, and may require confirmation with a full 3-dimensional model. Another proposed explanation has been invoked : that this phenomenon is a cloud produced from the evaporation of methane ice at the South Pole (Ref???)

It may require more long-term observations and follow-up of this occurrence before we fully comprehend its nature.

References

B´ezard, B. , Coustenis, A & McKay, C. P., 1995. Titan's stratospheric temperature asymmetry: a radiative origin?, Icarus 113, 267-276.

B´ezard, B. , Coustenis, A., Fouchet, T. *et al.* , 2004. Cassini/CIRS Observations of Titan's Equatorial Region in the Submillimeter Spectral Range. 36th DPS meeting, #22.04 BAAS 36, 1119.

Blanc, M., Bolton, S., Bradley, J. *et al.* , 2002. Magnetospheric and Plasma Science with Cassini-Huygens. Space Sci. Rev., 104, 253-346.

Bouchez, A. H., Brown, M. E., Neyman, C. R. *et al.* , submitted. Ground-based visible adaptive optics observations of Titan's atmosphere and surface. Icarus,submitted.

Bouchez, A. H., 2003. Ph. D. Thesis

Bratsolis, M. & Sigelle, M., 2001. A spatial regularization method preserving local photometry for Richardson-Lucy restoration. A&A 375, 1120-1128.

Brown, M. E., Bouchez, A. H. & Griffith, C. A., 2002. Direct detection of variable tropospheric clouds near Titan's south pole. Nature 420, 6917, 7995-797.

Caldwell, J., Cunningham, C. C., Anthony, D. *et al.* , 1992. Titan: Evidence for seasonal change - A comparison of Hubble Space Telescope and Voyager images. Icarus 97, 1-9.

Chanover, N. J., Anderson, C. M., McKay, C. P. *et al.* , 2003. Probing Titan's lower atmosphere with acousto-optic tuning. Icarus, 163, 1, 150-163.

Clarke, J. T., Grard, J.-C., Grodent, D. *et al.* , 2005. Morphological differences between Saturn's ultraviolet aurorae and those of Earth and Jupiter. Nature, 433, 717-719.

Combes, M., Vapillon, L., Gendron, E. *et al.* , 1997. Spatially resolved images of Titan by means of adaptive optics. Icarus 129, 2, 482-497.

Conan, J. M., Fusco, T., Mugnier, L. *et al.*, 1998a. Deconvolution of adaptive optics images with imprecise knowledge of the point spread function: Results on astronomical objects. In *Astronomy with Adaptive Optics: Present Results and Future Programs, ESO/OSA Workshop, Sept. 1998, Sonthofen, Germany.*

Coustenis, A., Lellouch, E., Maillard, J. P. & McKay, C. P., 1995. Titan's surface: composition and variability from the near-infrared albedo. Icarus 118, 87-104.

Coustenis, A., & B´ezard, B., 1995. Titan's atmosphere from Voyager infrared observations. IV. Latitudinal variations of temperature and composition, Icarus 115, 126-140.

Coustenis, A., Gendron, E., Lai, O. *et al.* , 2001. Images of Titan at 1.3 and 1.6 μm with adaptive optics at the CFHT. Icarus, 154, 501.

Coustenis, A., Hirtzig, M., Lai, O. *et al.* , 2002. New Adaptive Optics images of Titan with CFHT/PUEO: Atmospheric and Surface features. 34th DPS Meeting, #22.11; BAAS 34, 881.

Coustenis, A., **????????** EGS03

Coustenis, A., Negrão, A., Schulz, B. *et al.* (2004). First glimpses of Titan in the 2.75 micron window. In preparation.

Coustenis, A., Hirtzig, M.., Gendron, E. *et al.* (2005a). Maps of Titan's surface from 1 to 2.5μm. Submitted.

Coustenis, A., Negrão, A., Salama, A. *et al.* (2005b). Titan's 3-micron spectral region from ISO high-resolution spectroscopy. Submitted.

Flasar, F. M., Samuelson, R. E., & Conrath, B. J., 1981. Titan's atmosphere: temperature and dynamics, Nature 292, 693-698.

Gendron, E., Coustenis, A., Drossart, P. *et al.* , 2003. VLT/NACO adaptive optics imaging of Titan. Astron.& Astroph., in press.

Gibbard, S. G., Macintosh, B. A., Max, C. E. *et al.* , 2001. 2-micron adaptive optics images of Titan from the W.M. Keck Telescope. 199th AAS Meeting, #63.07. BAAS 33, 1403.

Griffith, C. A., Owen, T. & Wagener, R., 1991. Titan's surface and troposphere, investigated with ground-based, near-infared observations. Icarus, 93, 362-378.

Griffith, C. A., Owen, T., Miller, G. A, & Geballe, T., 1998. Transient clouds in Titan's lower atmosphere, Nature 395, 575-578.

Griffith, C. A., Hall, J. L., & Geballe, T. R., 2000. Detection of daily clouds on Titan. Science 290, 509.

Griffith, C. A., Owen, T., Geballe, T. R. *et al.* , 2003. Evidence for the exposure of water ice on Titan's surface. Science 300, 5619, 628-630.

Hilico, J. C., Champion, J. P., Toumi, S. *et al.* , 1994. New analysis of the pentad system of methane and prediction of the (pentad-pentad) spectrum. J. Mol. Spectrosc. 168, 455-476.

Hourdin, F., Talagrand, O., Sadourny, R. *et al.* , 1995. Numerical simulation of the general circulation of the atmosphere of Titan. Icarus 117, 358-374.

Hourdin, F., Lebonnois, S., Luz, D. & Rannou P., 2004. Titan's stratosphere: what the composition tells us about winds", J. Geophys. Res., submitted.

Hutzell, W. T., McKay, C. P., & Toon, W. B.: 1993. Effects of time-varying haze production on Titan's geometric albedo, Icarus 105, 162-174.

Kostiuk, T., Fast, K. E., Livengood, T. A. *et al.* , 2001. Direct measurement of winds of Titan. Geophysical Research Letters 28, 2361-2364.

Lemmon, M. T., Karkoschka, E. & Tomasko, M., 1993. Titan's rotation: surface feature observed. Icarus 103, 329-332.

Lemmon, M. T., Karkoschka, E. & Tomasko, M., 1995. Titan's rotational light-curve. Icarus 113, 1, 27-38.

Letourneur, B., & Coustenis, A., 1993. Titan's atmosphere from Voyager 2 infrared spectra, Planet. Space Sci. 41, 593-602.

Lockwood, G. W., Lutz, B. L., Thompson, D. T., & Bus, E. A., 1986. The albedo of Titan, Astrophys. J. 303, 511-520.

Lorenz, R. D., Smith, P. H., Lemmon, M. T., & Karkoschka, E., 1997. Titan's North-South Asymmetry from HST and Voyager imaging: comparison with models and ground-based photometry, Icarus 127, 173-189.

Lorenz, R. D., Lemmon, M. T., Smith, P. H. & Lockwood, G. W., 1999. Seasonal change on Titan observed with the Hubble Space Telescope WFPC-2. Icarus 142, 391-401.

Lorenz, R. D., E. F. Young & Lemmon, M. T., 2001. Titan's smile and collar: HST observations of seasonal change 1994-2000. Geo. Res. Letters 28, 23, 4453-4456.

Luz, D., Civeit, T., Courtin, R. *et al.*, 2005. Characterization of the Zonal Wind Flow in the Stratosphere of Titan with UVES. In prep.

McKay, C. P., Pollack, J. B. & Courtin, R., 1989. The thermal structure of Titan's atmosphere. Icarus 80, 23-53.

Meier, R., Smith, B. A., Owen, T. C. & Terrile, R. J., 2000. The surface of Titan from NICMOS observations with the Hubble Space Telescope. Icarus 145, 462-473.

Momary, T. W., Baines, K. H., Buratti, B. J. *et al.*, 2004. Not So Titanic Winds: Cassini/VIMS Observations of Cloud Features in the Southern Hemisphere of Titan. 36th DPS meeting, #06.10.

Negrão, A., Coustenis, A., Lellouch, E. *et al.* , 2003. Titan's 3 micron window with ISO. BAAS.

Negrão, A., Coustenis, **????????** COSPAR 2004

Neubauer, F. M., Gurnett, D. A., Scudder, J. D. & Hartle, R. E., 1984. Titan's magnetospheric interaction. In 'Saturn", edited by T. Gehrels & M. S. Matthews, Univ. Arizona Press, 760-787.

Pollack, J. B. & McKay, C. P., 1985. The impact of polar stratospheric clouds on the heating rates of the winter polar stratosphere. J. Atmos. Sci. 42, 245-262.

Porco, C. C., Baker, E., Barbara, J. *et al.*, 2005. Imaging of Titan from the Cassini spacecraft. Nature, 434, 159.

Rages, K., & Pollack, J. B., 1980. Titan aerosols: optical properties and vertical distribution. Icarus 41, 119-130.

Rages, K.. Pollack, J. B. & Smith, P. H., 1983. Size estimates of Titan's aerosols based on Voyager high-phase-angle images. Journal of Geophysical Research 88, 8721-8728.

Rannou, P., Cabane, M., Chassefiere, E. *et al.* , 1995. Titan's geometric albedo: Role of the fractal structure of the aerosols. Icarus 118, 355-372.

Rannou, P., Hourdin, F., & McKay, C. P., 2002. A wind origin for Titan's haze structure. Nature 418, 853-856.

Rannou, P., McKay, C. P. & Lorenz, R. D., 2003. A model of Titan's haze of fractal aerosols constrained by multiple observations. Planet. Space Sci. 51, 963-976.

Rannou, P., Hourdin, F., McKay, C. P. & Luz, D., 2004. A coupled dynamics-microphysics model of Titan's atmosphere. Icarus 170, 443-462.

Rigaut, F., Salmon, D., Arsenault, R. *et al.* , 1998. Performance of the Canada-France-Hawaii Telescope adaptive optics bonnette. The Publications of the Astronomical Society of the Pacific 110, 744, 152-164.

Ringrose, T. J., Towner, M. C. & Zarnecki, J. C. Convective vortices on Mars: a reanalysis of Viking Lander 2 meteorological data, sols 1-60. Icarus 163, 78-87.

Roe, H. G., de Pater, I., Macintosh, B. A. & McKay, C. P., 2002a. Titan's clouds from Gemini and Keck adaptive optics imaging. ApJ 581, 2, 1399-1406.

Roe, H. G., de Pater, I., Macintosh, B. A. *et al.* , 2003b. Titan's atmosphere in late Southern spring observed with adaptive optics on the W. M. Keck II 10-meter telescope. Icarus 157, 1, 254-258.

Roe, H. G., de Pater, I. & McKay, C. P., 2004. Seasonal variation of Titan's stratospheric ethylene (C2H4) observed, Icarus 169, 440-461.

Saint-P´e, O. ,Combes, M., Rigaut, F. *et al.* , 1993. Demonstration of adaptive optics for resolved imagery of solar system objects - Preliminary results on Pallas and Titan. Icarus 105, 263.

Schaller, E. L., Brown, M. E., Bouchez, A. H., *et al.* (2004). Continuous Monitoring of Titan for Large Cloud Outbursts. 36th DPS meeting, #6.09. BAAS 36, 1076.

Smith, B. A., Soderblom, L. A., Beebe, R., *et al.* , 1981. Encounter with Saturn: Voyager 1 imaging results, Science 212, 163-182.

Smith, B. A., Soderblom, L. A., Batson, R., *et al.* , 1982. A new look at the Saturn system: the Voyager 2 images. Science 215, 504-537.

Smith, P. H.. Lemmon, M. T.. Lorenz, R. D. *et al.* , 1996. Titan's surface, revealed by HST imaging. Icarus 119, 336-349.

Sromovsky, L. A., Suomi, V. E., Pollack, J. B. *et al.* , 1981. Implications of Titan's North-South brightness asymmetry. Nature 292, 698-702.

Sromovsky, L. A., & Fry, P. M., 1989. The phase variation of Titan's brightness contrast: implied constraints on properties of haze particles, Bull. Am. Astron. Soc. 21, 959.

Tokano, T., Neubauer, F. M., Laube, M. & McKay, C. P. Three-Dimensional Modeling of the Tropospheric Methane Cycle on Titan. Icarus 153, 130-147.

Tomasko, M. G. & Smith, P. H., 1982. Photometry and polarimetry of Titan - Pioneer 11 observations and their implications for aerosol properties. Icarus 51, 65-95.

Toon, O. B., McKay, C. P., Griffith, C. A. & Turco, R. P., 1992. A physical model of Titan's aerosols. Icarus 95, 24-53.

Waite, J. H., Grodent, D., Jr., Mauk, B. M. *et al.* , 2000. Multispectral Observations of Jupiter's Aurora. Advances in Space Research, Volume 26, Issue 10, p. 1453-1475.

West, R. A.. Hart, H.. Simmons, K. E. *et al.* , 1983. Voyager 2 photopolarimeter observations of Titan. Journal of Geophysical Research 88, 8699-8708.

West, R. A.& Smith, P. H., 1991. Evidence for aggregate particles in the atmospheres of Titan and Jupiter. Icarus, 90, 330-333.

Young, E. F.. Rannou, P.. McKay, C. P. *et al.* , 2002. A three dimensional map of Titan's troposphere haze distribution based on Hubble Space telescope imaging. The Astron. J. 123, 3473-3486.

Convective vortices on Mars, Ringrose et al. 2003
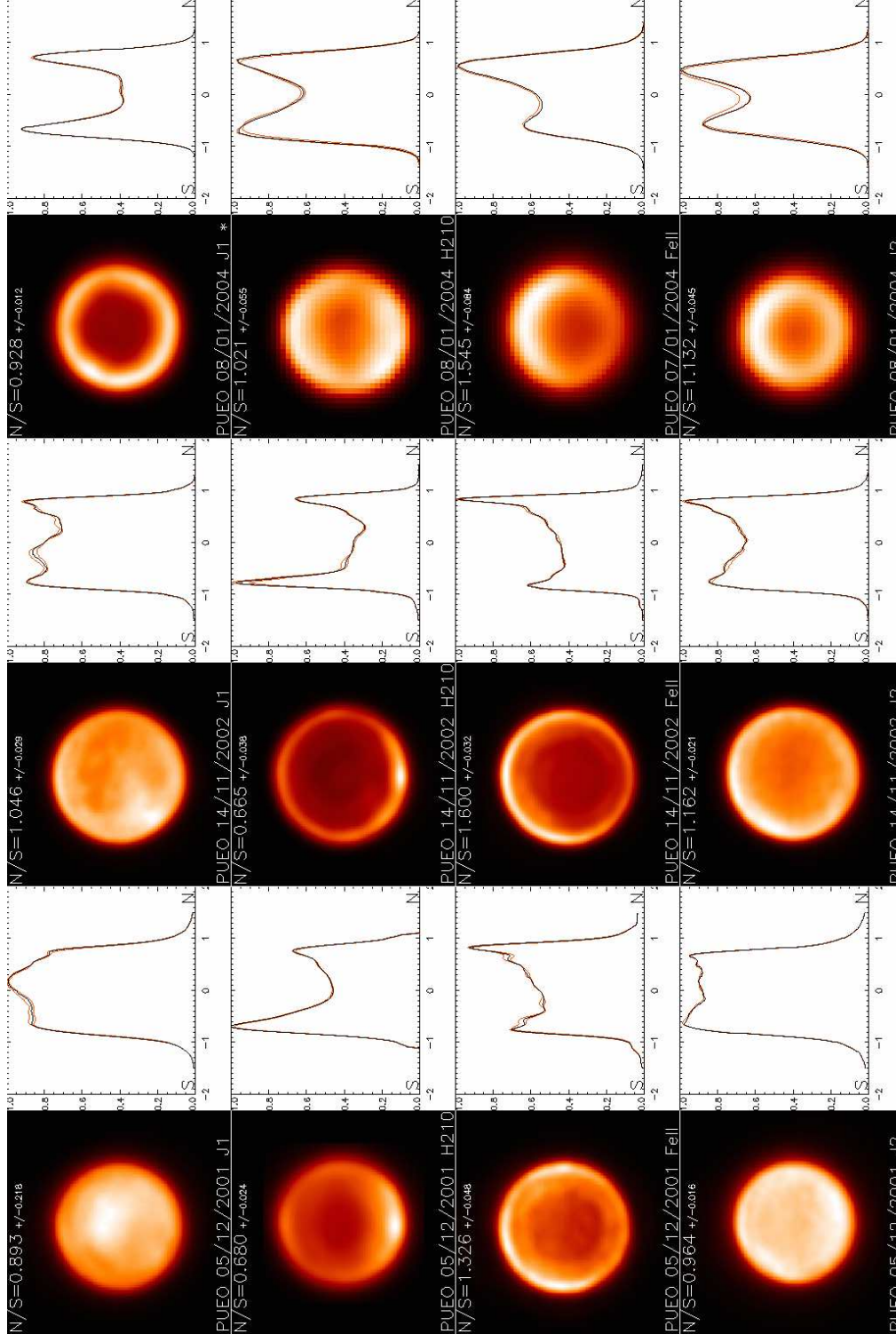
Fig. 1. Characteristic PUEO images showing the evolution of the North-South Asymmetry on Titan as a function of altitude in the atmosphere (different levels are probed in the atmospheric filters) and time. Altitude increases vertically, with the highest layers probed at the bottom and a surface filter (J1) at the top of the figure; time increases from Dec 2001 (left panel) to Jan 2004 (right panel). On each image, North is up, and West-map is to the left. The profiles drawn correspond to normalized intensity (1 being the brightest pixel of the whole image) from one limb to another. Error bars, shown in orange lines, correspond to variations from one resolution element to another. These profiles give us the North-South contrast with good precision, as indicated in the upper left corner of each sub-image.
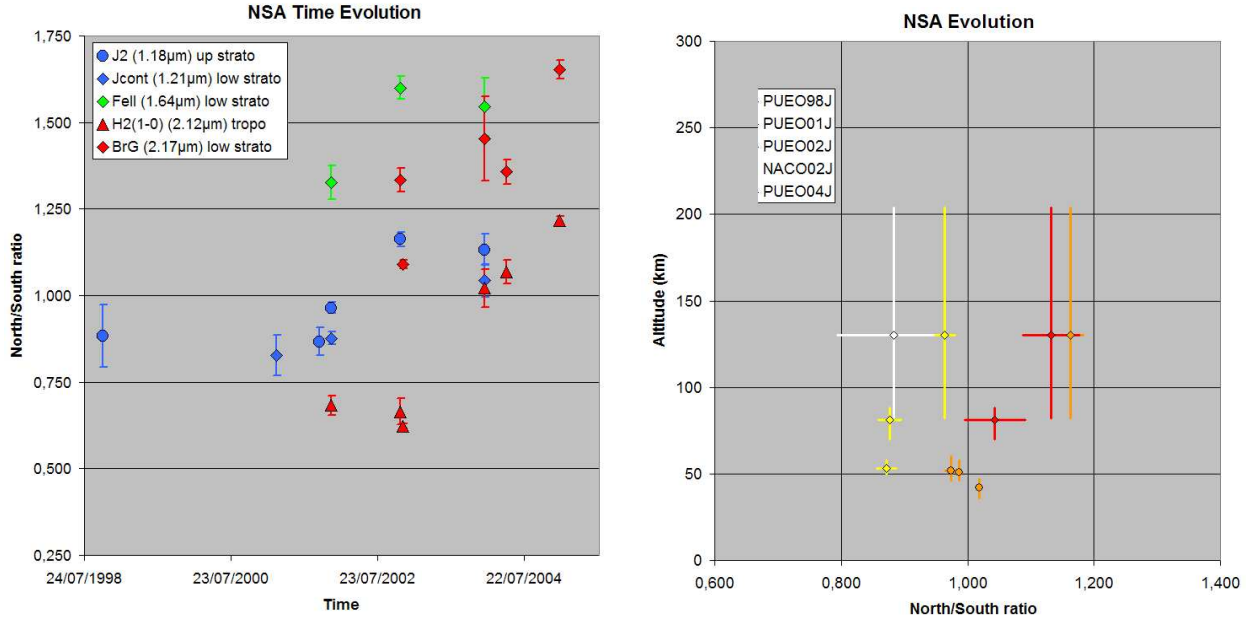
Fig. 2. Figure showing the evolution of the NSA over the past 7 years (1998-2005). Left panel: Time evolution of the NSA with characteristic filters (1.18, 1.21, 1.64, 2.12 and 2.17 micron). Color corresponds to wavelength (blue=J band, green=H band, red=K band), and symbol to altitude (triangle=troposphere, diamond=tropopause, circle=stratosphere). We show here both NACO and PUEO data when filters are equivalent (e.g. H2(1-0) and NB_2.12) Right panel : NSA evolution as a function of time and altitude, drawn only for J band filters for legibility ; the color code indicates the year of observation (white=1998, yellow=2001, orange=2002, red=2004) while the symbol reflects the instrument used (diamond=PUEO, circle=NACO).
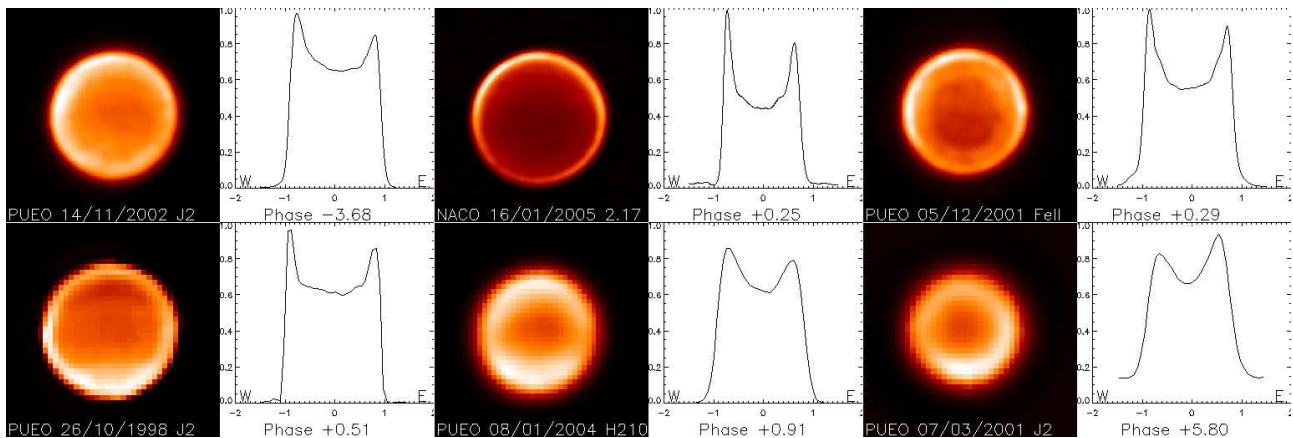
Fig. 3. Characteristic AO images showing the evolution of the East-West Asymmetry on Titan as a function of solar phase angle, regardless of the actual date of observation (reported on the bottom of each image, along with the instrument used and the solar phase angle value). From upper left to bottom right, the solar phase angle increases, showing the reversal of the phase effect from the morning (west, left) to the evening (east, right) side. The profiles drawn correspond to normalized intensity (1 being the brightest pixel of the image) from one limb to another, along one parallel, the one where the effect is maximum returning the nominal value reported in Table 3. At large phase angle values, the brightest limb corresponds to the one lit by the sunlight: western at negative phase angles (upper left), eastern at positive angles (bottom right). Yet at low phase angles (the four intermediate cases : upper center, upper right, bottom left and bottom center), the western limb (morning side) is always brighter than the eastern one (evening side), characteristic of a "morning fog" phenomenon related to a nocturnal condensation of stratospheric aerosols. See text and Coustenis et al. (2001) for details.
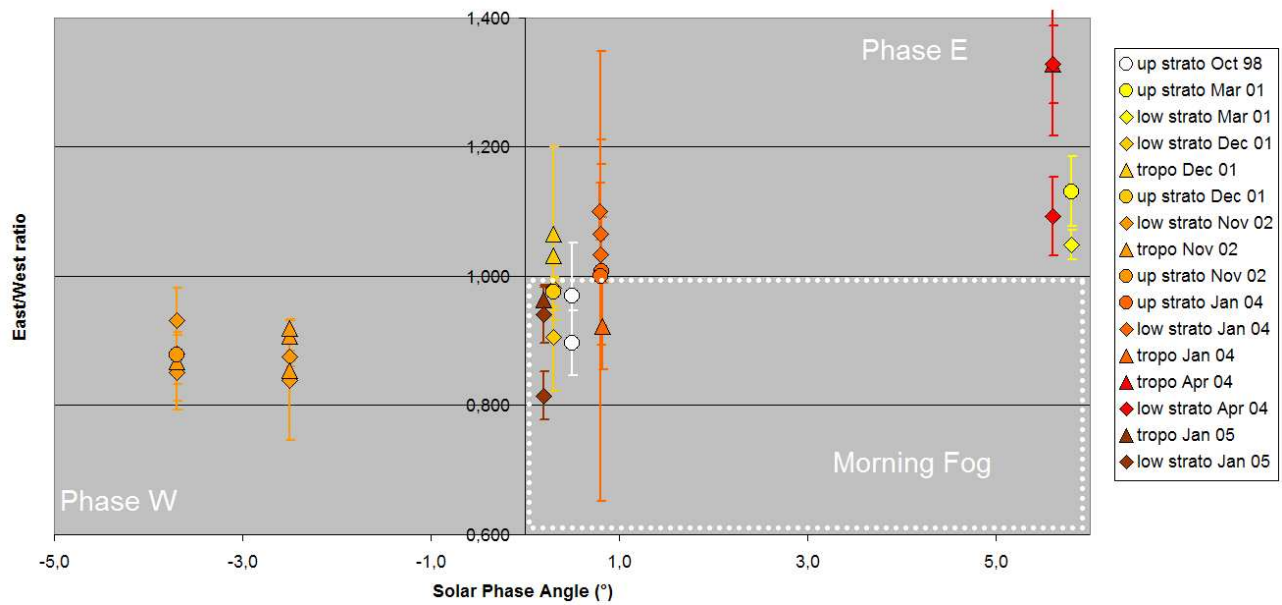
Fig. 4. Evolution of the EWA as a function of solar phase angle. Symbolism is similar to that used in Fig. 2: color indicates the year of the observation (white=1998, yellow=2001, orange=2002, red=2004, brown=2005), and the symbol the altitude probed (triangle=troposphere, diamond=tropopause, circle=stratosphere). A datum in the bottom left corner of this plot corresponds to the regular phase effect detection expected for a West-lit diffusing object (phase effect on the morning limb), while in the upper right corner it corresponds to the regular phase effect on the East (evening) limb with a positive solar phase angle. A homogeneous diffusing atmosphere would display a linear curve reaching 1.0 at 0 phase angle, but this is not Titan's case. Seven occurrences show a bright Western limb at low positive solar phase angle (the smaller the phase, the greater the 'morning fog', reaching about 20% at most), in particular in Oct 98, Dec 01 and Jan 05. Our 'morning fog' firm detections are in the lower right quadrant.
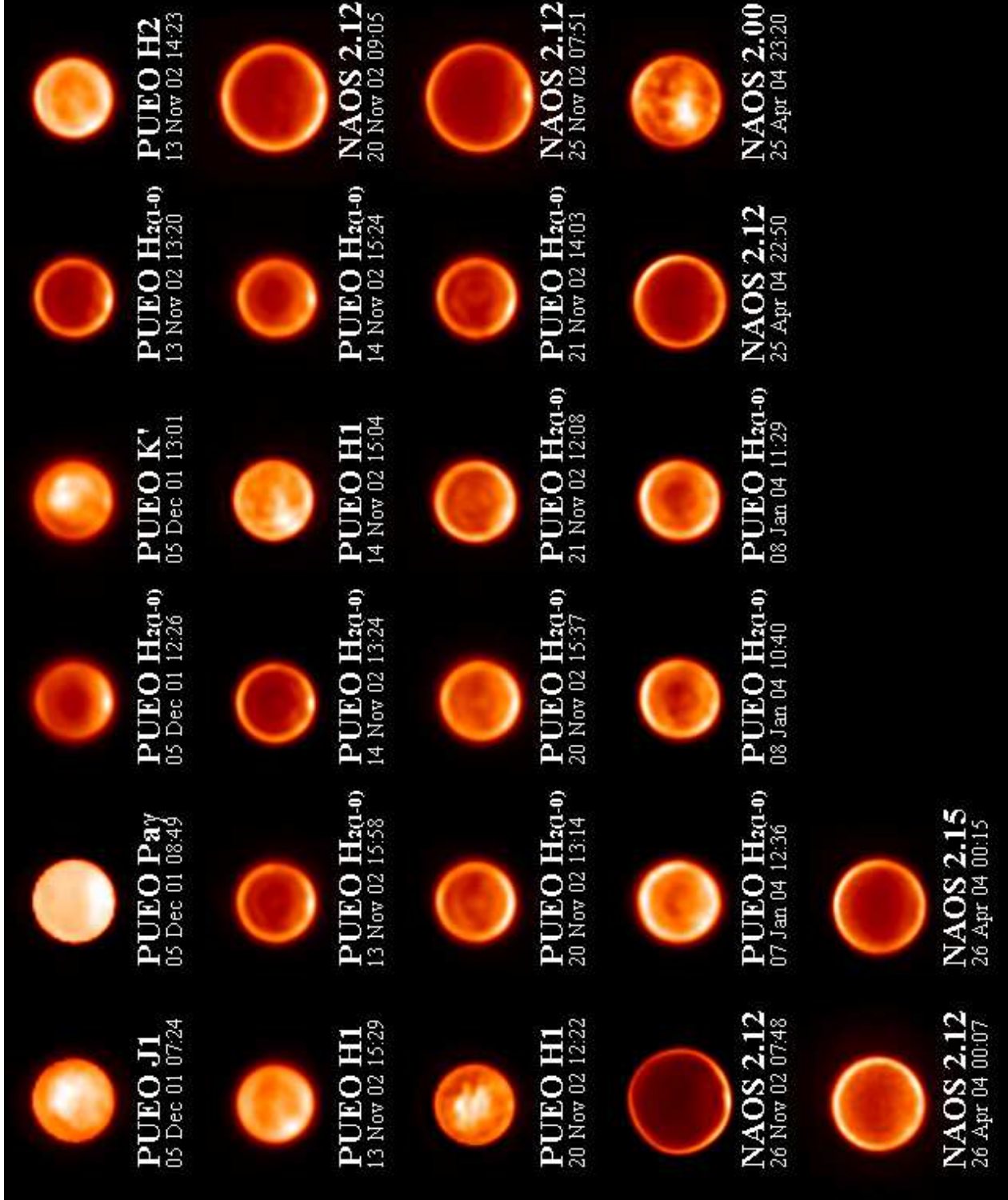
Fig. 5. Images in which we see the SPF, sorted in chronological order. In 2002 we observed this feature several times during the night of 20 Nov with both PUEO and NACO, and repeated this scheme as often as possible in 2004 runs. The feture is brighter in 2001 than in more recent years, because it was then enhanced by the bright southern limb of Titan.
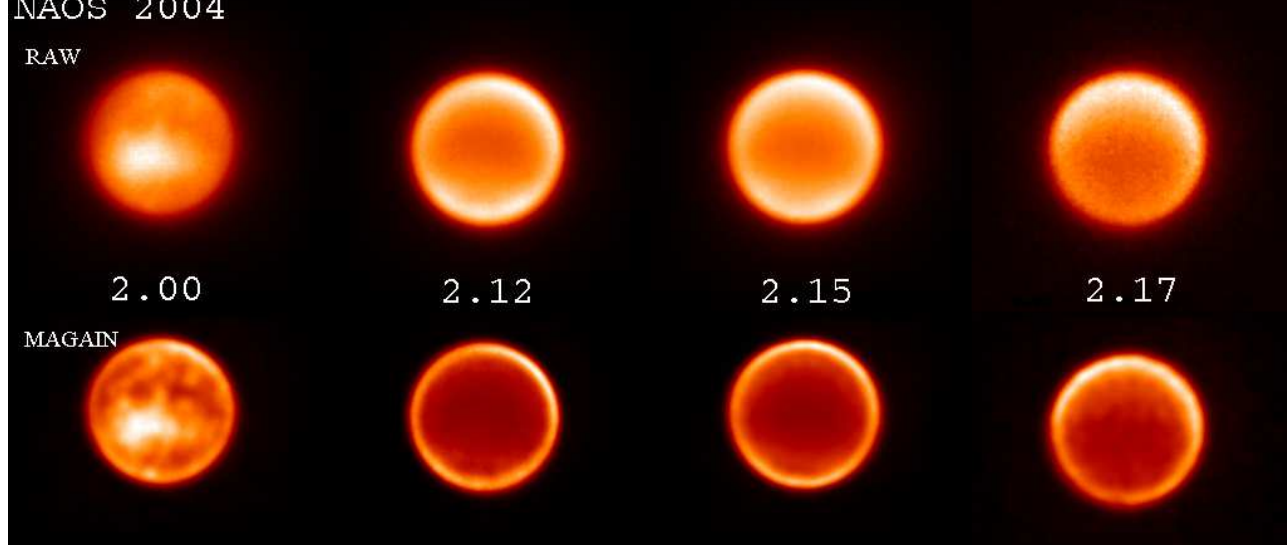
Fig. 6. Examples of detection and non-detection of the SPF in K band. The upper part displays the "raw" images before deconvolution, while the Magain-deconvolved ones lay on the bottom part. From left to right, images correspond to 2.00, 2.12, 2.15 and 2.17 micron 2004 NACO filters. When the SPF is present, it is bright on both (raw and deconvolved) images, but the two EPF and WPF companions only detach well from the SPF on the deconvolved image.
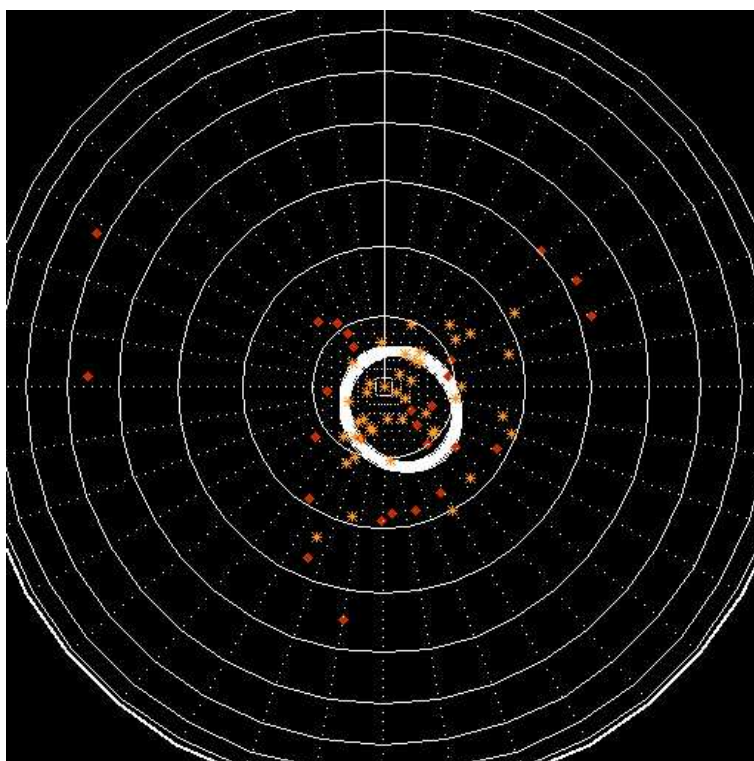

Fig. 7. Projections of the photocenter of the SPF on a spherical polar projection of Titan's Southern hemisphere (LCM=0° meridian is up). Yellow stars correspond to our detections, as detailed in Table 4. Red diamonds, extracted from Bouchez (2003) 1997-2003 data, are drawn for comparison only. The white ellipse corresponds to the region of maximum detection, overlapping half of the footprints shown here : 70% of them lay below the 80th parallel.